INTERCOMPARISON OF MODELS FOR CYGNSS DELAY-DOPPLER MAPS AT A VALIDATION SITE IN THE SAN LUIS VALLEY OF COLORADO

James D. Campbell[1], Ruzbeh Akbar[2], Amir Azemati[1], Alexandra Bringer[3], Davide Comite[4], Laura Dente[5], Scott T. Gleason[6], Leila Guerriero[5], Erik Hodges[1], Joel T. Johnson[3], Seung-Bum Kim[7], Amer Melebari[1], Nazzareno Pierdicca[4], Bowen Ren[8], Christopher S. Ruf[8], Leung Tsang[8], Haokui Xu[8], Jiyue Zhu[8], Mahta Moghaddam[1]

[1]University of Southern California, Los Angeles, CA 90007, USA
[2]Massachusetts Institute of Technology, Cambridge, MA 02139, USA
[3]Ohio State University, Columbus, OH 43210, USA
[4]La Sapienza University of Rome, Rome 00184, Italy
[5]University of Rome Tor Vergata, Rome 00133, Italy
[6]University Corporation for Atmospheric Research, Boulder, CO 80301, USA
[7]Jet Propulsion Laboratory, California Institute of Technology, Pasadena, CA 91109, USA
[8]University of Michigan, Ann Arbor, MI 48109, USA

ABSTRACT

A comparison of three different electromagnetic scattering models for delay-Doppler maps (DDMs) of global navigation satellite system reflectometry (GNSS-R) from land is performed along a Cyclone Global Navigation Satellite System (CYGNSS) track over a validation site in the San Luis Valley, Colorado, USA. The peak reflectivity profiles of all three models and of the corresponding CYGNSS data are found to be in general agreement and are strongly influenced by topography. An intercomparison of DDM structure for one acquisition is also included. Efforts to refine the model results using a high resolution lidar survey are ongoing.

***Index Terms*—** global navigation satellite system reflectometry (GNSS-R), land applications, scattering model, surface topography, Cyclone Global Navigation Satellite System (CYGNSS).

1. INTRODUCTION

Global navigation satellite system reflectometry (GNSS-R) over land surfaces is sensitive to a variety of geophysical parameters of interest for environmental monitoring. With the recent proliferation of satellite GNSS-R receivers, there is a growing need for the development and validation of electromagnetic scattering models to describe the delay-Doppler map (DDM) data generated by these sensors.

This work provides an initial intercomparison of DDM models for a Cyclone Global Navigation Satellite System (CYGNSS) [1] track over a validation site in the San Luis Valley (SLV), Colorado, USA. As the validation site has little vegetation, the intercomparison focuses on modeling the effects of topography, microwave-scale surface roughness, and soil dielectric constant. The intercomparison includes the following three DDM models:

1. An implementation of the fine-scale partially coherent patch (FPCP) method
2. The Soil And VEgetation Reflection Simulator (SAVERS)
3. An implementation of the improved geometrical optics with topography (IGOT) method

Each of these three models is based on the Kirchhoff integral, and each uses a different approximation for its evaluation.

2. SUMMARY OF MODELS

2.1. FPCP

In the FPCP approach [2], scattered fields are summed coherently over small to intermediate scales and incoherently over larger length scales. This approach is based on the fact that in random media, scattering can be coherent over small domains, but it becomes partially coherent in a domain of intermediate size and incoherent in a larger domain. To represent the land surface terrain, we use a 3-scale roughness model

$$f(x,y) = f_1(x,y) + f_2(x,y) + f_3(x,y)\,.$$

The $f_1(x,y)$ profiles are centimeter-scale microwave roughness, which was measured in-situ at CYGNSS cal/val sites.

The $f_3(x, y)$ profiles are obtained from the coarse-scale topography of a 30 m digital elevation map (DEM). We use these DEM elevations to construct 30 m tilted planar patches whose slopes are determined from the derivatives of $f_3(x, y)$. The $f_2(x, y)$ topography profiles are between the centimeter-scale microwave roughness and the 30 m coarse-scale DEM. Recently lidar measurements have been taken from which the fine-scale topography profiles can be reconstructed in the future. This fine-scale topography is important for the partially coherent model because in these intermediate-length scales, the scattered waves change from coherent to partially coherent to incoherent. In the present version of the partially coherent model, $f_2(x, y)$ is represented by adding a Gaussian random height of zero mean and a specified standard deviation to each small-scale patch, with the $f_2(x, y)$ value for each patch generated independently from all others.

The area is divided into sub-areas of $L^2_{\rm large}$. The $L_{\rm large}$ is chosen so that the scattered wave from $L^2_{\rm large}$ is incoherent, so that intensity summation rather than field summation can be carried out over different $L^2_{\rm large}$ areas. Within a single $L^2_{\rm large}$, we divide the surface into patches of area L^2, and $N_{\rm large} = L^2_{\rm large}/L^2$ is the number of patches in $L^2_{\rm large}$. In the present simulations, we use $L = 2\,{\rm m}$ and $L_{\rm large} = 30\,{\rm m}$ so that $N_{\rm large} = 225$. Each L^2 is a fine scale-patch with microwave roughness $f_1(x, y)$ superimposed on it. The fine-scale planar patch is added to the "patch height" $f_2(x, y)+f_3(x, y)$. Rough surface bistatic scattering theory is applied to compute fields for the L^2 patch. The resulting scattered waves for each patch consist of a coherent field and the incoherent diffuse scattered intensity. For the coherent wave, the complex field is kept with the amplitude and phase. The phase depends on the coordinates of the center of the patch. The coherent wave angular spread is described by a sinc function because of the finite L^2 patch size. The complex field summation is carried out over all small-scale patches within the large-scale patch area and then squared to obtain the intensity for that $L^2_{\rm large}$ area. Because of speckle associated with complex field summations, a Monte Carlo approach is used for the scattered intensities of $L^2_{\rm large}$ over realizations of $f_2(x, y)$. The resulting intensities for the $L^2_{\rm large}$ patches are then summed by addition of the diffuse intensities.

2.2. SAVERS

SAVERS is based on the original formulation in [3], which was designed to simulate low altitude receivers. It was updated as described in [4] to include the topography of the illuminated area, which cannot be neglected at satellite altitude. To account for topography, the DEM derived from the Shuttle Radar Topography Mission (SRTM) is considered. Each DEM element is a facet with its individual orientation, above which the roughness at wavelength scale is superimposed.

SAVERS implements the integral bistatic radar equation [5], independently evaluating the incoherent diffuse and coherent near-specular scattering components. The former is computed through the advanced integral equation method (AIEM), whereas the latter is simulated using the approach described in [6], which relies on the definition of a coherent normalized radar cross section (NRCS), associating a prescribed scattering pattern with the DEM facets.

SAVERS also includes a module for simulating vegetated areas, evaluating the scattering from forest and agricultural vegetation and setting the relevant geometric features of the vegetation elements through growth models. The modeling implements the radiative transfer equation, considering media constituted of randomly distributed scatterers representing different vegetation elements (namely, leaves, branches and trunks) [4]. The contributions of each DEM facet are combined through the radar equation considering the CYGNSS antenna pattern and the transformation between the local incidence and observation angles and polarization state going from the global reference frame linked to the instrument to the local facet reference frame and vice versa. In the work reported in this paper, the effects of vegetation are not included since the surfaces near the validation site were nearly bare at the time of data acquisition.

2.3. IGOT

The IGOT method, first described in [7], follows closely the approach of [5] with the assumption that the Rayleigh roughness parameter is large on the horizontal scale of the footprint of each delay-Doppler bin [8]. Unlike [5], however, the IGOT surface height is considered to be not a purely random field but rather decomposed into a deterministic part obtained from a DEM and a random part representing the residual height between the DEM and the surface. The random part of surface height is further decomposed into a longwave process and a shortwave process, following the improved geometric optics model of [9]. Thus, the IGOT model is parameterized by 1) DEM heights and gradients representing large-scale topography, 2) a root mean square (RMS) slope characterizing the roughness scale between the DEM resolution and the geometric optics cutoff, and 3) an RMS height accounting for attenuation due to shortwave diffraction.

3. DESCRIPTION OF VALIDATION SITE AND DATA

To support the calibration and validation of land applications for the CYGNSS mission, including retrieval of soil moisture and soil freeze-thaw state, two Soil moisture Sensing Controller and oPtimal Estimator (SoilSCAPE) in-situ wireless sensor networks (WSNs) were installed in the SLV of South Central Colorado in late October of 2019. Located at the headwaters of the Rio Grande, the SLV is generally flat and sandy with croplands being the dominant land cover. Each SoilSCAPE WSN includes multiple battery-powered end devices (EDs). Each ED has four probes to measure near real-

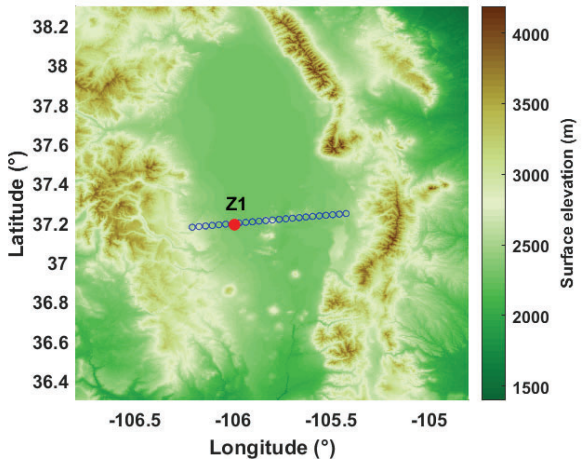

Fig. 1. Reported CYGNSS specular points of selected track (blue circles) and location of in-situ sensors at SLV site Z1 (red dot) plotted over a map of topography.

time soil moisture and soil temperature at depths of 5, 10, 20, and 30 cm [10].

As calibration of the SoilSCAPE soil moisture sensors requires collection of field samples through a range of soil moisture values and as these calibration activities have been delayed due to COVID-19 restrictions, soil moisture values from the October 2019 field samples were used for this study instead. After analysis of CYGNSS data near these field samples, the track around 2019-10-28 14:04:58.5 UTC from channel 3 of spacecraft 2 was selected for this study. This track, whose reported specular points are plotted over an elevation map in Fig. 1, passes over the SoilSCAPE validation site known as Z1 (37.190°, −105.992°). The start and end of the track were determined by requiring CYGNSS SNR to be greater than 2 dB.

All SoilSCAPE temperature sensors at Z1 indicated above-freezing soil temperatures for the selected track. The value of soil moisture from oven-drying of the Z1 field samples was 0.0259 m^3 m^{-3}. A laser range finder mounted on a horizontal bubble level supported by a tripod at each end was used to measure small-scale surface roughness along the 1 m baseline of the level at multiple locations around Z1. The corresponding values of RMS surface roughness ranged from 0.29 to 2.65 cm.

In addition to the approximately 30 m sampled SRTM DEM data shown in Fig. 1, an airborne lidar survey of these cal-val sites was conducted in 2020 that provided a DEM resolved at approximately 30 cm sampling and approximately 5 cm vertical uncertainty. The use of this fine-scale DEM for improving the description of medium-scale topography is currently in process. The impact of fine- to medium-scale topography on governing the interplay of coherent and incoherent contributions [8] is one of the important physical effects that may impact differences between model predictions.

4. RESULTS AND DISCUSSION

A comparison of peak reflectivity along the selected track is shown in Fig. 2. All three models used the 1″ SRTM DEM having approximately 30 m horizontal sampling for elevation. The models also used a common set of gradients estimated from the 1″ SRTM DEM using a 15-by-15 sample window. The FPCP and IGOT models both ran at the 1″ resolution of the SRTM DEM, while SAVERS resampled to a spacing of 9″, or approximately 300 m.

All three models used a soil dielectric constant of $3.293 + 0.198\,\mathrm{i}$ from a soil moisture of 0.025 m^3 m^{-3} based on the field samples described in Section 3 and a clay fraction of 20 % following [11]. The models also used a value of 1 cm for the microwave-scale surface roughness. The FPCP model used a value of 5 cm for patch height randomization in f_2. The IGOT model was run with a relative RMS slope of 0.4°. All three models used an isotropic antenna pattern.

The two most recent versions of CYGNSS level 1 science data are included for comparison. Although version 3.0 has the advantage of addressing GPS flex power events by including dynamic calibration of effective isotropic radiated power, version 3.0 also introduces an unintended bias in the receiver antenna patterns, which will be resolved in version 3.1. For this reason, version 2.1 may be more accurate than version 3.0 over SLV, as North America is generally unaffected by GPS flex power events.

As seen in Fig. 2, all three models generally follow the reflectivity profile of the CYGNSS data, which is highest over the valley floor and decreases in the mountainous terrain on either side and to a lesser extent over some hilly terrain in the middle. The profile of the models is seen to be smoother than that of the data. This is potentially due to the relatively large window that was needed to filter out noise when estimating gradients from the SRTM DEM. Ongoing work includes investigation of the use of the lidar survey to improve model fidelity, particularly over the patch of terrain in the middle of the valley floor. We also note that the bias of each model can be reduced by adjusting the corresponding microwave-scale surface roughness parameter. Additional in-situ characterization of this parameter is needed.

A comparison of DDMs for the acquisition closest to site Z1, which has time of 2019-10-28 14:04:58.5 UTC and reported specular point coordinates of (37.197°, −106.003°), is shown in Fig. 3. Good agreement in structure is seen among all four DDMs for the near-specular delay-Doppler bins. Although the models appear to have more power for the bins located around the edges than the data, these edge differences are in fact small due to the logarithmic scale of the plot. As a final observation, all DDMs exhibit a tail at positive Doppler. Tails have also been observed with TechDemoSat-1 [4], and analysis indicates that the observed Doppler asymmetries arise from structures in the underlying topography.

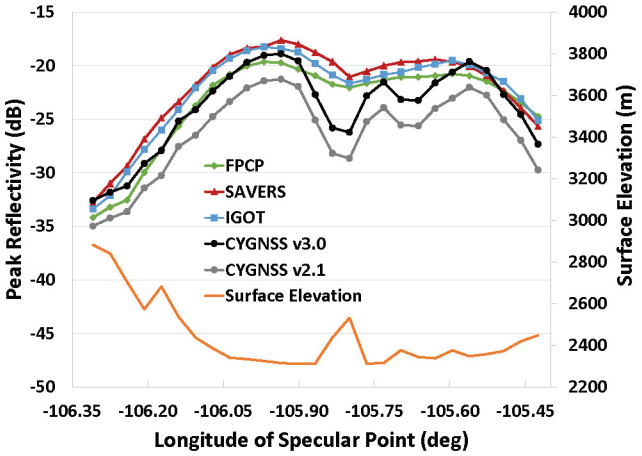

Fig. 2. Comparison of peak reflectivity from the three models and from two versions of corresponding CYGNSS level 1 science data along the selected track.

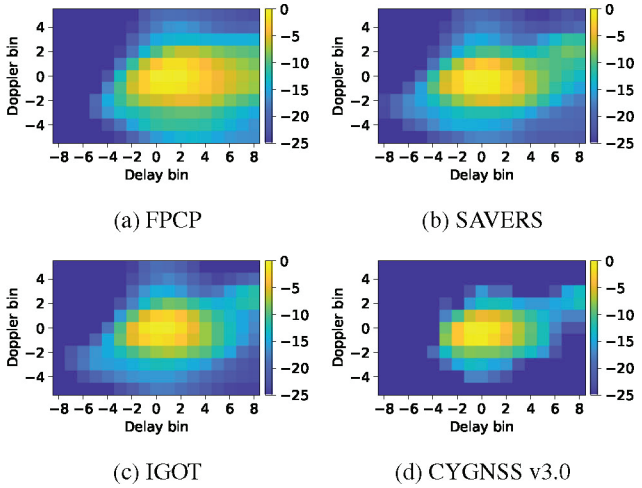

Fig. 3. Comparison of DDMs from the three models and from the corresponding CYGNSS level 1 science data for the selected acquisition. Each DDM is normalized to its peak value to facilitate intercomparison of delay-Doppler structure.

References

[1] C. S. Ruf, C. Chew, T. Lang, M. G. Morris, K. Nave, A. Ridley, and R. Balasubramaniam, "A new paradigm in earth environmental monitoring with the CYGNSS small satellite constellation," *Scientific Reports*, vol. 8, no. 1, Jun. 2018. DOI: 10.1038/s41598-018-27127-4.

[2] H. Xu, J. Zhu, L. Tsang, and S. B. Kim, "A fine scale partially coherent patch model including topographical effects for GNSS-R DDM simulations," *Progress In Electromagnetics Research*, vol. 170, pp. 97–128, 2021. DOI: 10.2528/pier20121201.

[3] N. Pierdicca, L. Guerriero, R. Giusto, M. Brogioni, and A. Egido, "SAVERS: A simulator of GNSS reflections from bare and vegetated soils," *IEEE Trans. Geosci. Remote Sens.*, vol. 52, no. 10, pp. 6542–6554, Oct. 2014. DOI: 10.1109/tgrs.2013.2297572.

[4] L. Dente, L. Guerriero, D. Comite, and N. Pierdicca, "Space-borne GNSS-R signal over a complex topography: Modeling and validation," *IEEE J. Sel. Topics Appl. Earth Observ. Remote Sens.*, vol. 13, pp. 1218–1233, 2020. DOI: 10.1109/jstars.2020.2975187.

[5] V. U. Zavorotny and A. G. Voronovich, "Scattering of GPS signals from the ocean with wind remote sensing application," *IEEE Trans. Geosci. Remote Sens.*, vol. 38, no. 2, pp. 951–964, 2000. DOI: 10.1109/36.841977.

[6] D. Comite, F. Ticconi, L. Dente, L. Guerriero, and N. Pierdicca, "Bistatic coherent scattering from rough soils with application to GNSS reflectometry," *IEEE Trans. Geosci. Remote Sens.*, vol. 58, no. 1, pp. 612–625, Jan. 2020. DOI: 10.1109/tgrs.2019.2938442.

[7] J. D. Campbell, A. Melebari, and M. Moghaddam, "Modeling the effects of topography on delay-Doppler maps," *IEEE J. Sel. Topics Appl. Earth Observ. Remote Sens.*, vol. 13, pp. 1740–1751, 2020. DOI: 10.1109/jstars.2020.2981570.

[8] A. M. Balakhder, M. M. Al-Khaldi, and J. T. Johnson, "On the coherency of ocean and land surface specular scattering for GNSS-R and signals of opportunity systems," *IEEE Trans. Geosci. Remote Sens.*, vol. 57, pp. 10 426–10 436, 2019. DOI: 10.1109/TGRS.2019.2935257.

[9] D. R. Thompson, T. M. Elfouhaily, and J. L. Garrison, "An improved geometrical optics model for bistatic GPS scattering from the ocean surface," *IEEE Trans. Geosci. Remote Sens.*, vol. 43, no. 12, pp. 2810–2821, Dec. 2005. DOI: 10.1109/tgrs.2005.857895.

[10] R. Akbar, J. D. Campbell, A. R. Silva, R. Chen, A. Melebari, E. Hodges, D. Entekhabi, C. S. Ruf, and M. Moghaddam, "SoilSCAPE wireless in situ networks in support of CYGNSS land applications," in *IEEE International Geoscience and Remote Sensing Symposium (IGARSS)*, to appear, Jul. 2020.

[11] V. Mironov, Y. Kerr, J.-P. Wigneron, L. Kosolapova, and F. Demontoux, "Temperature- and texture-dependent dielectric model for moist soils at 1.4 GHz," *IEEE Geosci. Remote Sens. Lett.*, vol. 10, no. 3, pp. 419–423, May 2013. DOI: 10.1109/lgrs.2012.2207878.